Plasma flows and fluctuations with magnetic islands in the edge of J-TEXT tokamak

K. J. Zhao,[1, 2, 3] Y. J. Shi,[1, 3, 4] S. H. Hahn,[1, 3] P. H. Diamond,[1, 5] Y. Sun,[6] J. Cheng,[2] H. Liu,[6] N. Lie,[2] Z. P. Chen,[6] Y. H. Ding,[6] Z. Y. Chen,[6] B. Rao,[6] M. Leconte,[1] J. G. Bak,[3] Z. F. Cheng,[6] L. Gao,[6] X. Q. Zhang,[6] Z. J. Yang,[6] N. C. Wang,[6] L. Wang,[6] W. Jin,[6] L. W. Yan,[2] J. Q. Dong,[2] G. Zhuang,[6] and J-TEXT team

1. WCI Center for Fusion Theory,
NFRI, Gwahangno 113, Yusung-gu, Daejeon 305-333, Korea
2. Southwestern Institute of Physics, P. O. Box 432, Chengdu, China
3. National Fusion Research Institute,
Gwahangno 113, Yusung-gu, Daejeon 305-806, Korea
4. University of Science and Technology of China, China
5 Center for Momentum Transport and Flow Organization,
University of California at San Diego, California 92093, USA
6. College of Electrical and Electronic Engineering,
Huazhong University of Science and Technology, Wuhan Hubei, 430074, China

Abstract: The first comprehensive measurements of plasma flows and fluctuations nearby static magnetic islands driven by resonant magnetic perturbations (RMPs) are presented. These experiments were performed using multiple Langmuir probe arrays in the edge plasmas of the J-TEXT tokamak. The effects of controlled variations of the island size and location are explored. This study aims to understand the interaction between turbulence and magnetic islands, and to elucidate magnetic island effects on edge turbulence and flow intensity profiles, edge electric fields, and thus confinement regime transitions. Turbulence and low frequency flows (LFFs) all drop inside the magnetic island, but increase at its boundary, as island width increases. The geodesic acoustic mode (GAM) is damped in most of the edge area with magnetic islands. The sign of the radial electric field changes from negative to positive within

the islands. The gradient of turbulent stresses vanishes at island center, and becomes steeper at the boundary of the islands. The particle transport induced by the turbulence is reduced inside the magnetic islands. The magnetic island effects on flows and turbulence can lead to an increase in LFFs and enhance Reynolds stresses near the last closed flux surface (LCFS). A stronger radial electric field layer can be formed near the LCFS when magnetic islands are present. The results suggest that magnetic islands can be used as a tool to enhance edge turbulence and flows, edge electric fields, and thus to trigger confinement regime transitions.

1. Introduction

Interaction of magnetic field structures and flows is a subject of general interest in physics. Typical examples include magnetic braking of stellar rotation [1], angular momentum transport in astrophysical disks [2, 3], and dynamics of the earth core and geodynamo [4]. In fusion plasmas, the study of interactions between turbulent fluctuations and magnetic islands aims to understand and control plasma confinement and transport. Magnetic islands have significant effects on the profiles and cross field transport [5–8], and can grow to large amplitudes and lead to disruptions [9].

Evidence suggests that there is a link between the strength of **EXB** flow shear near the location of rational surfaces and the presence of magnetic islands [10]. The latter may contribute to the formation of an internal transport barrier [11, 12]. External resonant magnetic perturbations (RMPs) can generate not only stochastic magnetic fields, but also coherent magnetic islands [13]. RMP-induced stochastic regions have strong effects on turbulence [14–17]. The common feature with stochastic layers is that the radial electric field E_r near the LCFS increases. The radial electric field is also influenced by magnetic islands [18-20]. However, the impact of magnetic islands on zonal flows and turbulence has not been studied although this is a crucial issue because of its relevance to confinement regime transitions [21-23].

The zonal flows in magnetically confined plasmas are defined as azimuthally symmetric radial electric field fluctuations. Two types of ZFs in toroidal plasmas have been identified, namely the low-frequency zonal flows (LFZFs) [24-26] and the geodesic acoustic modes

(GAMs) [27, 28] of frequency, $\omega_{\mathrm{GAM}} = \sqrt{\gamma(T_i + T_e)/M_i}$ /R, where γ is the adiabatic index, T_i and T_e are ion and electron temperature, respectively, M_i and R are ion mass and major radius of the torus, respectively. The LFZF was proved to contribute to the transition from low confinement mode (L-mode) to high confinement-mode (H-mode) [29-32]. Note that previous studies of RMP effects on turbulence have been focused on stochastic layers, not coherent islands.

Here, we present the first observation of low frequency flows (LFFs) enhanced by the presence of magnetic islands. The self-consistent evolutions of the turbulence-flow system in the presence of magnetic islands of controllable width and location are described. The LFFs and turbulence drop inside the magnetic island, but increase at its boundary, as island width increases. The LFF, Reynolds stress, and radial electric field E_r near the last closed flux surface (LCFS) are enhanced when magnetic islands approach the LCFS.

The rest of this work is organized as follows. The experimental set-up is given in section 2. The experimental results, described in section 3, include island effects on the radial electric fields, turbulence, flows, power spectra of floating potential fluctuations, and particle transport induced by turbulence, etc. Section 4 presents the conclusion and discussion.

2. Experiment setup

The experiments presented here were conducted in Ohmic plasmas with circular cross section on the J-TEXT tokamak. The major and minor radii of the J-TEXT tokamak are R = 1.05 m and a = 0.255 m, respectively [33]. The plasma parameters for the experiments are the toroidal magnetic field B_t = 1.5-2.0 T, the plasma current I_p = 150-180 kA, the line averaged electron density N_e = 1-3X$10^{19}m^{-3}$, and the edge safety factor q_a = 3.2-4.3. A set of coils, called a dynamic RMP, has been installed inside the vessel on J-TEXT to study the interaction between helical perturbations and magnetized plasmas, and explore a possible method for control of tearing modes [34]. In the present study, the static configuration of RMP was used. The base mode and strength of the magnetic perturbation were varied by adjusting the power supply to the coils. The perturbation field strength of B_r ~0.542 Gs for m/n = 3/1 mode, and of ~0.116 Gs for m/n = 4/1 mode can be obtained for 1kA in the coils

assuming no plasma response. Here, m and n are the poloidal and toroidal mode numbers, respectively. The maximum RMP current is 6.5 kA. A combination of distributed Langmuir probe (LP) arrays was employed. In this combination, a fast reciprocating probe array with two steps and 12 tips as shown in the figure 1 (a) yields the profiles of floating potential, temperature, density, Mach number, etc. A radial rake probe array of 12 tips presented in the figure 1(b) was used to get the radial profiles of the floating potential to study plasma flow structure [35]. They were mounted on the top of the tokamak. The length and diameter of the tips are 3 mm and 2 mm, respectively. The digitizer can handle fluctuation data up to 2 MHz.

3. Experimental results

3.1. Radial profiles of radial electric fields and fluctuations with 4/1 islands

Magnetic islands are detected in the edge plasmas with q_a = 4.3 when RMP coils are applied. The RMP current is 5kA and produces a relative magnetic perturbation $B_r/B_0 \sim 3 \times 10^{-5}$ for the m/n = 4/1 mode, as calculated without considering the plasma response. Here, B_0 is the main magnetic field. The radial dependences of the edge electron temperature and radial electric field with (red circles) and without (blue squares) RMPs are given in figures 2 (a)-(b). Compared with the case without RMPs, the shape of the electron temperature profile is much different. T_e is flattened inside the islands [5]. At the island boundary of ~1.5 cm inside the LCFS, T_e becomes steeper. The island width is estimated as ~1.0 cm from the temperature profiles. The flattening T_e and half of the steep boundary were considered for this estimation. With islands, the radial electric field changes from negative to positive inside the islands, and decreases from Δr = -0.5 to 0 cm near the LCFS. Here, Δr means the distance from the measurement position to the LCFS and minus means inside the LCFS. The decrease of E_r in the interval Δr = -0.5 to 0 cm differs from the measurements in the case with a stochastic boundary [14-16]. The decrease of E_r near the LCFS means the E_r layer becomes stronger. E_r is derived from the radial derivative of the plasma potential. The plasma potential can be estimated from the measured temperature (T_e) and floating potential (ϕ_f) as $\phi_{pl} \sim \phi_f + 2.5T_e$.

Turbulence response to magnetic islands is examined. The root mean square amplitude of the floating potential fluctuations in the frequency band of 30-400 kHz is provided in the figure 3 (a). Turbulence intensity drops significantly, by up to 30%, inside the magnetic island,

and increases at its boundary. The radial profiles of the weighted average of the poloidal wave number k_θ for the turbulence are also shown in the figure 3 (b). The k_θ is calculated by the cross-phase analysis. The negative k_θ inside the LCFS indicates that the turbulence propagates in the electron diamagnetic direction. But in the island regime, the k_θ increases and its sign changes from negative to positive. The positive k_θ suggests that the turbulence moves in the ion diamagnetic direction. The effects of magnetic islands on turbulence are consistent with theoretical expectation, i. e., inside magnetic islands, turbulence drops and propagates in the ion diamagnetic direction [35].

To understand the interaction of magnetic islands with turbulence, turbulent Reynolds stress and its gradient are measured and presented in figures 4 (a) and (b). The Reynolds stresses are estimated as $< \delta v_r \delta v_\theta >$, here, δv_r and δv_θ are the radial and poloidal turbulent velocities, computed from the high frequency components of the turbulence. < ... > is the time average over a time period of ~2 ms. The δv_r (δv_θ) is estimated by floating potential fluctuations from tips at two poloidal (radial two) positions, assuming that the temperature fluctuations can be neglected in low temperature plasmas. Two negative bumps of Reynolds stresses appear with RMPs. One is localized at the LCFS and the other occurs in the magnetic island region. The negative bump in the magnetic island region suggests that flows are driven there. The negative (positive) gradients of Reynolds stresses correspond to positive (negative) E_r near the LCFS with and without RMPs. The E_r profiles are shown in figure 1(b). The steeper gradient of Reynolds stresses corresponds to stronger E_r. These indicate that the Reynolds stresses are correlated with E_r. In contrast, the gradient of Reynolds stress is zero at the island center, and becomes steeper at the island boundary. The reversal of the gradient of Reynolds stress suggests that the sign of turbulence-driven flows reverses at the island center. The positive E_r in the magnetic island region does not agree well with the measurement of the Reynolds stresses. This suggests the positive E_r formation is due to a direct effect of the islands. The more negative bump and steeper gradient of Reynolds stresses near the LCFS with RMPs suggest that the Reynolds stresses are enhanced by the presence of magnetic islands. The enhanced Reynolds stresses drive stronger E_r and enhance sheared flows. This is consistent with measurement of the E_r, i.e., E_r decreases near the LCFS with magnetic islands. The island effects on sheared flow structure will be discussed further.

3.2. Radial profiles of radial electric fields and fluctuations with 3/1 islands

Magnetic islands are also detected in the edge plasmas with q_a = 3.3 when RMP coils are applied. The RMP current is 6 kA and produces a relative magnetic perturbation $B_r/B_0 \sim 2 \times 10^{-4}$ for the m/n = 3/1 mode without considering the plasma response. The radial profiles of the edge electron temperature and radial electric field with and without RMPs are presented in figures 5(a)-(b). Similarly, T_e is flattened inside the islands while at the island boundary of Δr ~-1.5cm, T_e becomes steeper with RMPs. With islands, the sign of the radial electric field also changes from negative to positive inside the islands, but E_r increases from Δr = -0.5 to 0 cm near the LCFS. The increase of E_r with 3/1 islands does differ from that with 4/1 islands, where the E_r decreases. The island width is estimated as ~1.0 cm. Compared with the cases without islands, the electron temperatures decrease in most of the edge area.

The root mean square amplitude of the floating potential fluctuations in the frequency band of 30-400 kHz is provided in the figure 6 (a). With 3/1 islands, the shape of turbulence intensity profile is similar to that with 4/1 islands, i. e, the turbulence level is lower (higher) inside islands (at the island boundary). In contrast with the case without islands, the turbulence intensity significantly drops near the LCFS with 3/1 islands. This differs from that with 4/1 islands, where the turbulence intensity increases near the LCFS. Figure 6(b) shows the radial profiles of the weighted average of the poloidal wave number k_θ for the turbulence with and without 3/1 islands. There are no significant differences between 3/1 and 4/1 island effects on the poloidal wave numbers of turbulence.

Turbulent Reynolds stress and its gradient are presented in figures 7 (a) and (b). Two negative bumps of Reynolds stresses appear with islands again. The gradient of Reynolds stress is consistent with the measurement with the cases with 4/1 islands, i. e., the gradient of turbulent stresses becomes steeper at the boundary of the islands and its sign reverses at the island center. However, the less negative bump and lower gradient of Reynolds stresses near the LCFS with 3/1 islands suggest that the Reynolds stresses can also be damped in the presence of magnetic islands.

3.3 Effects of resonant layers on edge electron temperature and radial electric fields

Figures 8 (a)-(b) show the radial profiles of the electron temperature and radial electric field (E_r) , respectively, with edge safety factor scan. The positions of the resonant layers were varied through adjusting the edge safety factor. The plasma current was kept at ~150 kA, and the q_a values ~3.8, 4.1 and 4.3 were obtained by varying the magnetic field B_T ~1.8, 1.9 and 2.0 T. The RMP current is 5 kA. The islands appear at q_a=4.3. No significant islands are observed in the edge region with q_a=3.8. The radial profiles of T_e and E_r at q_a=3.8 are similar to those observed in the cases without RMPs. With q_a~4.1, the positive E_r regime also occurs in the interval $-1.2 < \Delta r < -0.2$ cm. Compared with q_a=4.3, the electron temperature and E_r profiles are significantly different. The flattened T_e disappears in the interval $-1.2 < \Delta r < -0.2$ cm although the T_e drops there. The E_r becomes fattened near the LCFS, i.e., increases inside the LCFS and decreases outside the LCFS. Note that the edge E_r is similar to the measurement with a stochastic layer. Thus, the significant difference at q_a = 4.1 might come from a stochastic layer formation because the resonant flux surface is closer to the LCFS. The results suggest that there are significant differences between the effects of magnetic islands and of stochastic regions on edge plasma parameters, and thus turbulence and flows.

3.4. Radial structures of flows with magnetic islands

Figure 9 presents the auto power spectra of the floating potential fluctuations with and without islands at Δr ~-2.0 cm. The island width and the edge safety factor are the same as shown in the figure 1. Two distinct features are a large power fraction in the low frequency range 0–4 kHz and a sharp peak at f ~16 kHz. The frequency resolution is 0.5 kHz. The former is called a LFF in this paper because of no measurements of poloidal and toroidal mode numbers although it has already been identified as a LFZF in the cases without island on other machines [27, 28]. Without island, the calculated radial and poloidal wave vectors for the sharp peak are k_r ~2.4 cm^{-1} and k_θ ~0.0 cm, respectively. With islands, k_θ is zero and k_r is about 3.2 cm^{-1}. This is consistent with the theory prediction of GAMs. 提供参考文献 The ambient turbulence (AT) is mainly located in the frequency bands of 30-100 kHz. With islands, turbulence and LFF intensity increases while the GAM drops.

The island effects on the power spectra of the floating potential fluctuations were studied further. Figures 10 (a)-(d) provide the power spectra of the floating potential fluctuations with

and without 4/1 islands at the positions of inner boundary of the islands, inside islands, outer boundary of the islands, and in SOL. The island width is ~1 cm and q_a=4.3. The GAM is observed at the inner boundary of the islands. With islands, the GAM is damped and its frequency increases to ~25 kHz. The LFF and turbulence drop inside the islands and increase at their boundaries. In the SOL regime, turbulence intensity almost does not change due to far away from the islands. In this analysis, the frequency resolution is ~ 1 kHz.

The power spectra of the floating potential fluctuations with and without 3/1 islands at several positions are presented in the figures 11(a)-(d). The island width and q_a are ~1.6 cm and 3.5, respectively. Without islands, a large power fraction in the GAM frequency of ~19 kHz are detected inside the LCFS. With islands, the GAM drops at all the positions and its frequency also moves to a higher frequency ~24 kHz. The LFF drops inside the islands and increases at their boundaries. This is similar to that with 4/1 islands. The turbulence intensity decreases inside the islands and increases at its outer boundary. At the inner boundary, the reduction of turbulence intensity is not consistent with the measurements with 4/1 islands as shown in figure 10(a). Compared with the case with 4/1 islands, there is no significant difference for the turbulence intensity in the SOL regime.

Figures 12 (a)-(c) give the radial profiles of GAM power in the frequency band of ~15-30 kHz, LFF power in the frequency range of 0.3-3 kHz, and root mean square amplitudes of floating potential fluctuations in the frequency band of 30-400 kHz, with and without RMPs. With RMPs, the GAM power decreases in most of the edge region and the reduction of GAM intensity is more pronounced inside magnetic islands. The shapes of LFF power and turbulence intensity profiles are much more complicated with magnetic islands. The LFF power and turbulence intensity have a local minimum inside the islands, and get higher values at their boundary. Without islands, the LFF power and turbulence intensity tend to increase inward [36]. In contrast with the case without islands, the LFF power increases at the boundaries of the islands while turbulence intensity just increases at the outer boundary of the magnetic islands.

The dependence of LFFs and turbulence on the island size is also investigated using an RMP coil-current scan. Figures 13 (a) and (b) present the radial profiles of LFF powers and root mean square amplitudes of floating potential fluctuations. Without RMPs, the LFF power

and turbulence intensity also tend to increase inward. The width of m/n = 3/1 islands increases from 1.6 to 3.2 cm while increasing the RMP current from 2 to 4 kA. The reduction of LFF power and turbulence intensity inside the magnetic island is clearly shown again. However, at the outer boundary of the magnetic island, the LFF power and turbulence intensity both increase for increasing the RMP current. The most interesting observation is that the islands lead to an increase in LFF and turbulence near the LCFS. This might be useful in controlling transitions.

3.5. Radial wave numbers of turbulence with magnetic islands

The spectrum of radial wave numbers of the turbulence is examined with and without magnetic islands. Figure 14 provides the weighted average of radial wave numbers of turbulence with and without RMPs. The radial wave numbers are estimated with two point correlation techniques [37]. Based on the wave number-frequency spectrum $S(k,f)=1/M\sum_{i=1}^{m} I[k-k_i(f)]S_{crs,i}(f)$, the spectral averaged wave number can be derived. Here, $I\ (a-b)$ = 1 if $a = b$, otherwise, $I\ (a-b)$ = 0, $S_{crs,i}(f)$ and M represent the cross-correlation function and the number of realizations, respectively. The shapes of the radial wave number profiles of turbulence with islands differ from those observed in the case without islands. With islands, the values of the radial wave numbers of turbulence are higher inside the islands. This is because that the GAM is damped in the presence of islands, so GAM shearing and the associated convection cells are eliminated. Without islands, the higher values appear at ~1.6 cm. The radial wave numbers in the interval -1.2 <Δr < 0 cm are smaller with islands than those measured in the case without islands.

3.6. Particle transport induced by turbulence with magnetic islands

The particle transport induced by turbulence with 4/1 magnetic islands at q_a=4.3 is estimated with calculating $<\delta I_s \delta E_\theta>$. The island width is ~1 cm. Here, the δI_s and δE_θ are saturated ion current fluctuations and poloidal electric field fluctuations, respectively. Figure 15 shows the radial profiles of $<\delta I_s \delta E_\theta>$ with and without islands. $<\delta I_s \delta E_\theta>$ is reduced

inside the magnetic islands due to the decrease in fluctuation amplitudes. No negative particle fluxes were detected in the present experiment. This distinguishes the results from the observations in the stochastic region on TEXTOR [14, 15]. The $< \delta I_s \delta E_\theta >$ also decrease slightly near the LCFS.

The $< \delta I_s \delta E_\theta >$ near the LCFS is examined further with 3/1 magnetic islands at q_a=3.5 during RMP modulation. Figures 16 (a)-(d) show the time evolutions of the RMP current, saturated ion fluctuation, poloidal electric fluctuation and $< \delta I_s \delta E_\theta >$. The probe position is ~0.5 cm inside the LCFS and island width is about ~2.4 cm with RMPs. With RMPs, the saturated ion fluctuation and the $< \delta I_s \delta E_\theta >$ drop significantly. But the δE_θ almost does not change. This suggests that the reduction of $< \delta I_s \delta E_\theta >$ may come from the decrease in saturated ion fluctuation amplitude.

4. Conclusion and discussion

The plasma flows and fluctuations with static, RMP-driven islands were studied using multiple Langmuir probe arrays in the edge of the J-TEXT tokamak. Some common features are observed. The electron temperature is flattened inside the islands, and become steeper at their boundaries. The fluctuation level is lower inside the islands and higher at the island boundaries. The sign of the E_r changes from negative to positive inside the islands. The gradient of turbulent Reynolds stresses becomes steeper at the boundaries of the islands and its sign reverses at the island center. The geodesic acoustic mode is damped in most of the edge area with magnetic islands. In some cases, the island effects can lead to the enhancement of the LFF, E_r and Reynolds stresses near the LCFS. The intensity of turbulence and LFFs drops inside the magnetic island, but increases at its boundary, as island size increases. The gradient of turbulent stresses can become steeper near the LCFS with magnetic islands. A stronger E_r shear layer is formed when magnetic islands move towards the LCFS. However, opposite effects of islands on the radial electric fields, and turbulence are also detected near the LCFS, i.e., the intensity of turbulence and the negative E_r decrease near the LCFS with magnetic islands.

The observations of the flat Te profiles and the lower fluctuation level inside the islands

are consistent with the theoretical expectation [9]. The enhancement of the LFF, E_r and Reynolds stresses near the LCFS with magnetic islands was not detected in the previous observations with a stochastic layer. The negative particle transport with stochastic layers does not appear with magnetic islands. In this experiment, the flows and turbulence are measured in one toroidal location. For better understanding of the interaction between islands and turbulence, three dimensional effects of islands on the edge flows and turbulence should be studied in the future. Moreover, the variety of island effects on turbulence and flows near the LCFS are not understood in the current stage.

The most interesting observation is the enhancement of the LFF, E_r and Reynolds stress near the LCFS with magnetic islands. Bursty Reynolds stresses and LFZFs were found during limit cycle oscillations [38], and confirmed to induce L-H transitions [29-32]. The predator-prey oscillations depend on the magnetic configuration on TJ-II, i.e. on the order of the rational surface located at the plasma edge [39]. Magnetic islands with a suitable width do not deteriorate the confinement significantly, but enhance the LFFs and Reynolds stresses near the LCFS. This is favorable to lower the L-H threshold power or trigger confinement regime transitions. Thus, we speculate that magnetic islands near the LCFS may promote enhanced confinement (i.e. such as the L-H transition) by causing the formation of edge peaked Reynolds stress and LFF profiles, which enhance shearing and hasten the collapse of turbulence. In particular, increasing the peaking of Reynolds stress profiles approaching the LCFS may lower the L-H threshold power and/or allow access to other enhanced regimes. Future work will focus the use of variable magnetic islands to control confinement regimes in general, and the L-H transition, in particular.

Acknowledgments: We are grateful to Profs. K. Itoh, G. R. Tynan, A. Fujisawa, S. Inagaki, Y. Nagashima, and A. J. Wootton for helpful discussions. This work is supported by the WCI Program of the National Research Foundation of Korea funded by the Ministry of Education, Science and Technology of Korea [WCI 2009-001]; by the fund of State Key Laboratory of Advanced Electromagnetic Engineering and Technology in HUST [2015KF00*]; by National Science Foundation of China, Nos. 11175060, 11175058, 11375054, 91130031, 11320101005 and 11075046; by the National Magnetic Confinement Fusion Science Program

No.2013GB107001, 2014GB107000 and 2013GB112008; by the U.S. Department of Energy (DOE) under Award Number DE-FG02- 04ER54738 and CMTFO; and by Fundamental Research funds for Central Universities, China-Korean joint foundation under the Grant No. 2012DFG02230.

References

[1] Seanp Matt, et al., APJ, **754**, L26 (2012).

[2] Balbus S A and Hawley J F, APJ, **376**, 241(1991).

[3] Balbus S A and Hawley J F, Rev. Mode. Phys, **70**, 1 (1998).

[4] Aubert J and Fournier A, Nonlin. Processes Geophys, **18**, 657 (2011).

[5] Suttrop W et al., Nucl. Fusion **37**, 119 (1997).

[6] Fiksel G et al., Phys. Rev. Lett.**75**, 3866 (1995).

[7] Inagaki S et al., Phys. Rev. Lett. **92**, 055002 (2004).

[8] Ida K et al., Phys. Rev. Lett. **88**, 015002 (2001).

[9] Biskamp D, Magnetic Reconnection in Plasmas, (Cambridge University Press, Cambridge, England, 2000).

[10] Hidalgo C et al., Plasma Phys. Cont. Fusion, **42**, A153-A160 (2000).

[11] Ida K et al., Phys. Rev. Lett. **109**, 065001 (2012).

[12] Estrada T et al, Nucl. Fusion, **47**, 305 (2007).

[13] Jakubowski M W et al., Phys. Rev. Lett. **96**, 035004 (2006).

[14] Xu Y et al., Phys. Rev. Lett. **97**, 165003 (2006).

[15] Xu Y et al., Nucl. Fusion, **47**, 1696 (2007).

[16] P Tamain et al., Plasma Phys. Control. Fusion **52**,075017 (2010).

[17] Leconte M and Diamond P H, Phys. Plasmas **19**, 055903 (2012).

[18] O. Bondarenko, et al.,Contrib. Plasma Phys. **55**, 605 (2010).

[19] D. López-Bruna, et al., Plasma Phys. Control. Fusion **53**, 124022 (2011).

[20] K. Ida et al., Nuclear Fusion **44,** 290 (2004).

[21] Diamond P H et al., Plasma Phys. Cont. Fusion, **47**, R35 (2005).

[22] Hasegawa A et al., Phys. Rev. Lett. **59**, 1581(1987).

[23] Conway G D et al., Phys. Rev. Lett. **106**, 065001(2011).

[24] Fujisawa A et al., Phys. Rev. Lett. **93** 165002 (2004).

[25] Liu A D et al., Phys. Rev. Lett. **103** 095002 (2009).

[26] Miki K et al., Phys. Plasmas **19**, 092306 (2012).

[27] Zhao K J et al., Phys. Rev. Lett. **96** 255004 (2006).

[28] McKee G R et al., 2003 Phys. Plasmas **10** 1712 (2003).

[29] Manz P et al., Phys. Plasmas **19**, 072311(2012).

[30] Tynan G et al., Nucl. Fusion **53**, 073053 (2013).

[31] Cziegler I et al., Plasma Phys. Cont. Fusion , **56**, 075013 (2014).

[32] Yan Z et al., Phys. Rev. Lett. **112**, 125002 (2014).

[33] Zhuang G et al., Nucl. Fusion, **51**, 094020 (2011).

[34] Rao B, et al., Fusion engineering and design, **89**, 378 (2014).

[35] Fitzpatrick. R, Phys. Plasmas **2**, 825 (1994).

[36] Zhao K J et al., Nucl. Fusion, **53**, 083011 (2013).

[37] Beall J M et al., J. Appl. Phys. **53**, 3933 (1982).

[38] Zhao K J et al., Nucl. Fusion, **53**, 123015 (2013).

[39] Estrada T et al., Europhys. Lett. **92,** 35001 (2010).

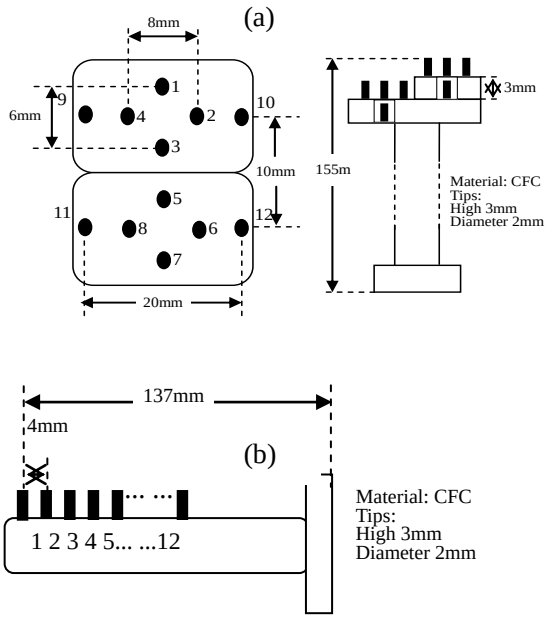

Figure. 1 (color online) Configurations of (a) fast reciprocating probe array and (b) radial rake probe array.

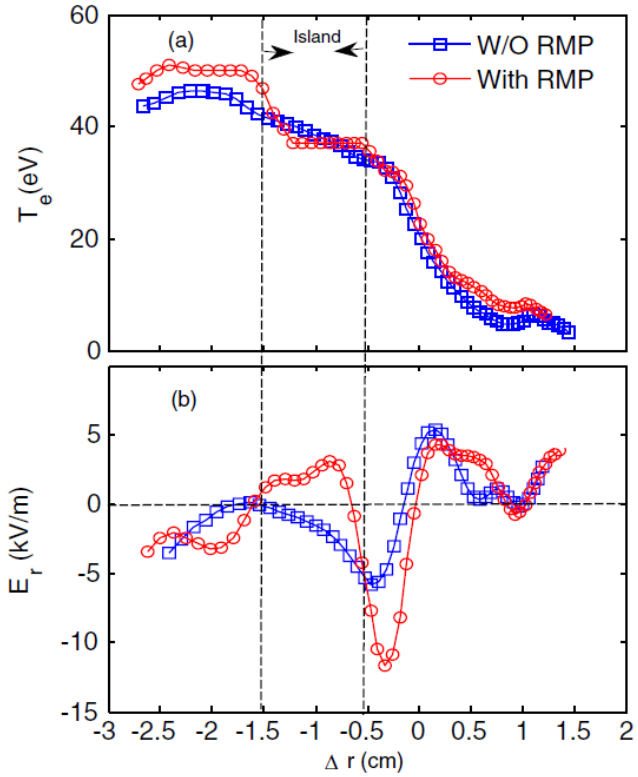

Figure. 2 (color online) Profiles of edge plasma parameters and fluctuations without (blue squares) and with (red circles) RMPs, (a) electron temperature, (b) radial electric field (E_r). ($\omega_{i,*}$ and $\omega_{e,*}$ refer to ion and electron diamagnetic directions, respectively, N_e~2.2x$10^{19}m^{-3}$, B_t~2.0T, I_p~150kA, I_{rmp}~5kA, m/n=4/1 island).

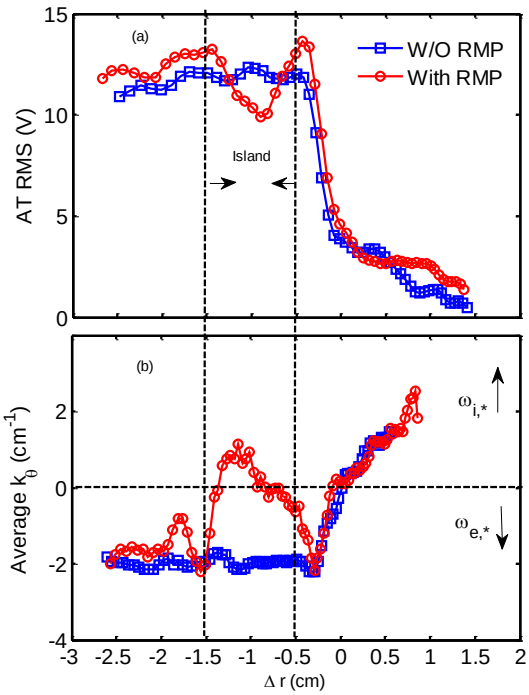

Figure. 3 (color online) Radial profiles of turbulence intensity (a) and averaged poloidal wave-vector (b) without (blue squares) and with (red circles) RMPs (N_e~2.2x$10^{19}m^{-3}$, B_t~2.0T, I_p~150kA, I_{rmp}~5kA, m/n=4/1island).

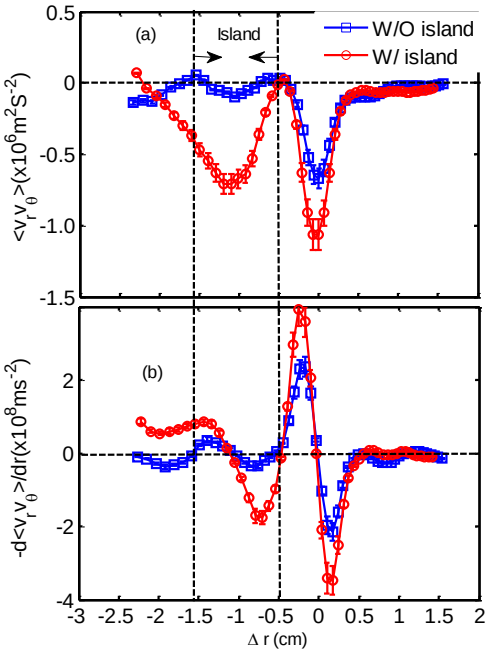

Figure. 4 (color online) Profiles of (a) turbulent Reynolds stress and (b) its gradient with and without magnetic islands. (N_e~2.2x$10^{19}$$m^{-3}$, B_t~2.0T, I_p~150kA, I_{rmp}~5kA, m/n=4/1island)

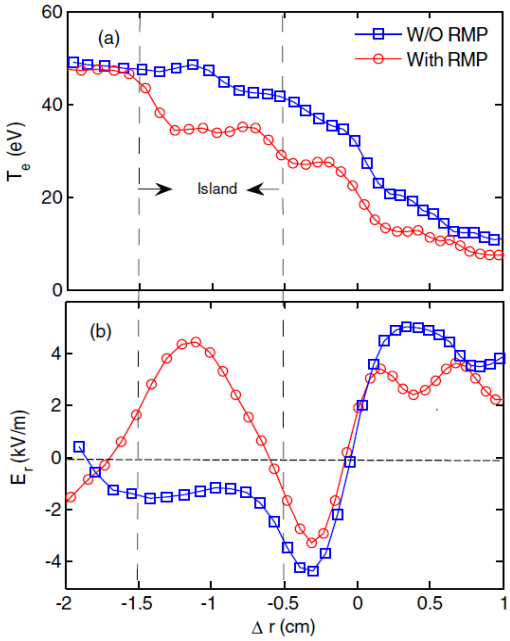

Figure. 5 (color online) Profiles of edge plasma parameters and fluctuations without (blue squares) and with (red circles) RMPs, (a) electron temperature, (b) radial electric field (E_r). (N_e~3.2x10^{19}m^{-3}, B_t~1.6T, I_p~160kA, I_{rmp}~6kA, m/n=3/1 island).

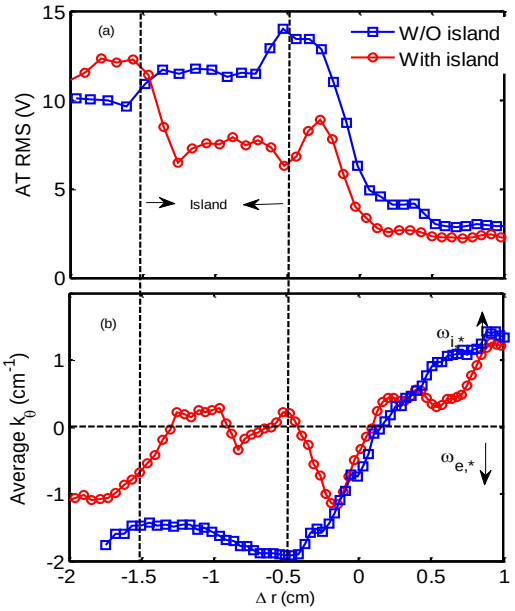

Figure. 6 (color online) Radial profiles of turbulence intensity (a) and averaged poloidal wave-vector (b) without (blue squares) and with (red circles) RMPs (N_e~3.2x10^{19}m^{-3}, B_t~1.6T, I_p~160kA, I_{rmp}~6kA, m/n=3/1 island).

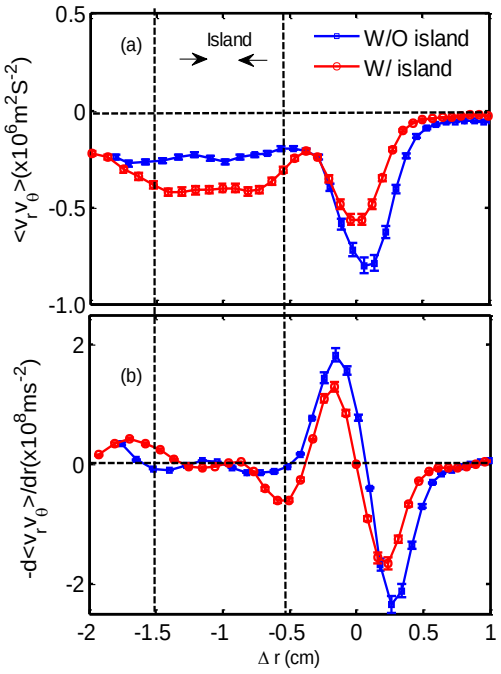

Figure. 7 (color online) Profiles of (a) turbulent Reynolds stress and (b) its gradient with and without magnetic islands. (N_e~$3.2x10^{19}m^{-3}$, B_t~1.6T, I_p~160kA, I_{rmp}~6kA, m/n=3/1 island)

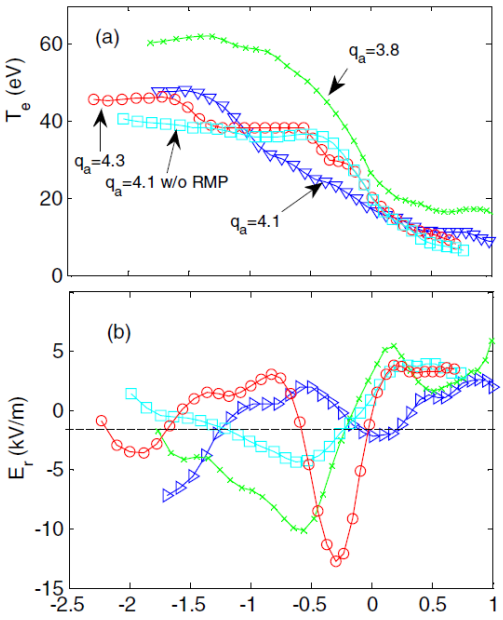

Figure. 8 (color online) Profiles of edge plasma parameters with edge safety factor scan and 4/1 RMP current of 5kA, (a) electron temperature, (b) radial electric field (E_r) (N_e~2.2x$10^{19}$$m^{-3}$, I_p~150kA, B_t~1.8, 1.9, 2.0T).

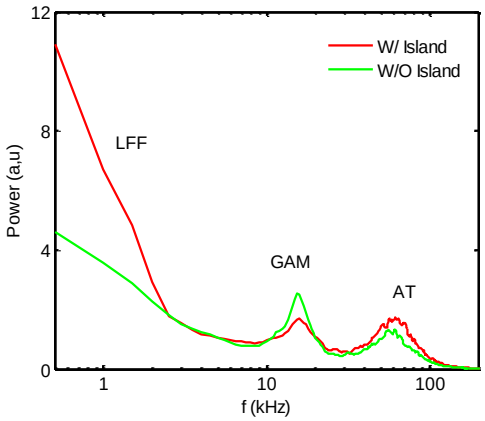

Figure. 9 (color online) Auto-power spectra of the floating potential fluctuations at Δr ~-2.0 cm with and without islands. ($\overline{N}_e$ ~ 2.2 X$10^{19} m^{-3}$, I_p ~150 kA, B_t ~2.0 T, q_a~4.3, I_{rmp}=5 kA, m/n=4/1 island)

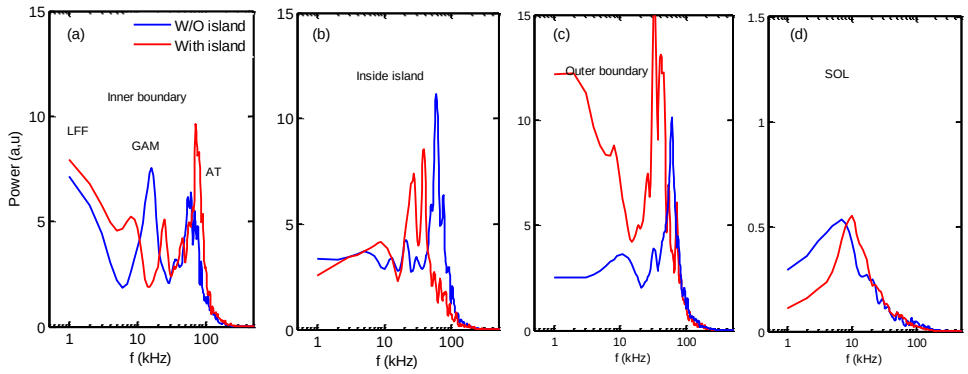

Figure. 10 (color online) Auto-power spectra of the floating potential fluctuations with and without islands. (Inner boundary Δr ~-1.5 cm, inside island Δr ~-1.0 cm, outer boundary Δr ~-0.5 cm, SOL Δr ~1cm, $\overline{N}_e$ ~ 2.2 X$10^{19}m^{-3}$, I_p ~150 kA, B_t ~2.0 T, q_a~4.3, I_{rmp}=5 kA, m/n=4/1 island)

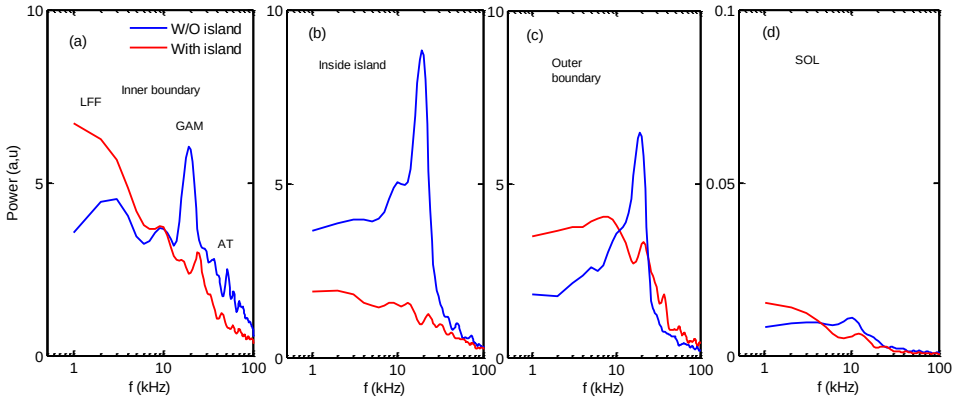

Figure. 11 (color online) Auto-power spectra of the floating potential fluctuations with and without islands. (Inner boundary Δr ~-3.0cm, inside island Δr ~-2.0cm, outer boundary Δr ~-1.7cm, SOL Δr ~1cm, $\overline{N}_e$ ~ 2.0 X$10^{19}m^{-3}$, I_p ~140 kA, B_t ~1.5T, q_a~3.5, I_{rmp}=3kA, m/n=3/1 island)

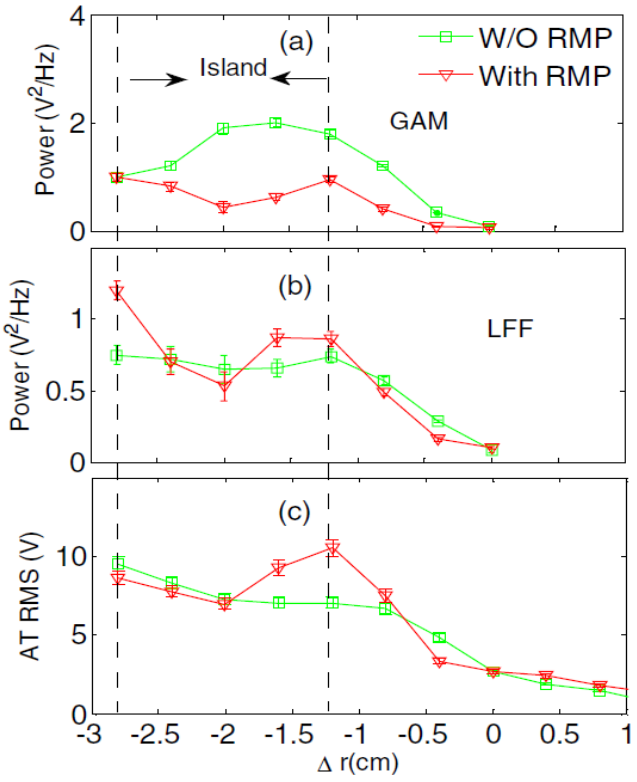

Figure. 12 (color online) The radial profiles of GAM power (a), LFF power (b), and root mean square amplitude of turbulence in the frequency band of 30-400kHz (c) with and without RMPs. ($\bar{N}_e$ ~ 2.0 X10$^{19}m^{-3}$, I_p ~140 kA, B_t ~1.5T, q_a~3.5, I_{rmp}=3kA, m/n=3/1 island).

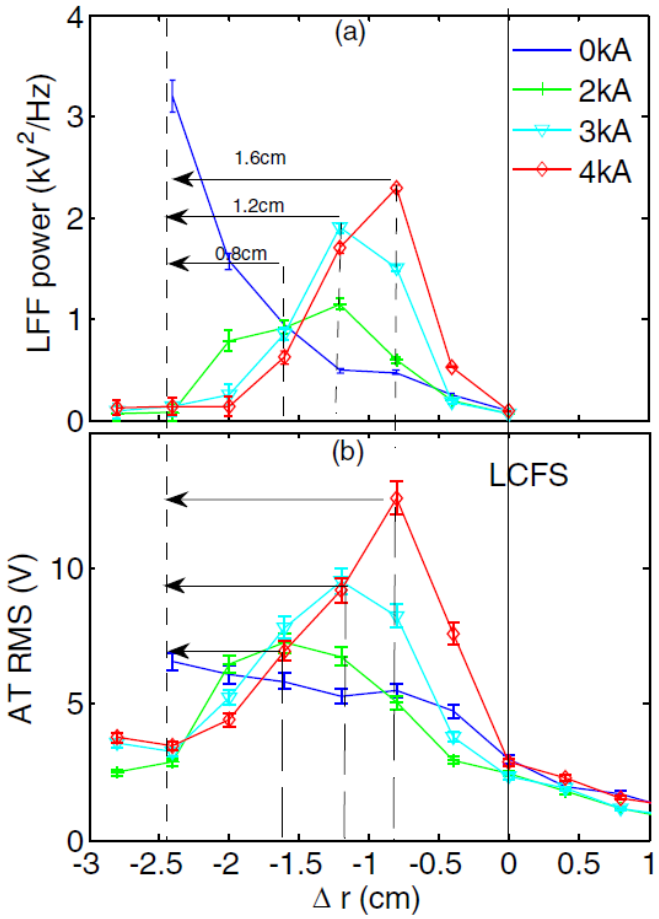

Figure. 13 (color online) The radial dependence of (a) LFF power, and (b) root mean square amplitudes of turbulence in the frequency band of 300-400 kHz, as island width increases. (The island centers are indicated by dash-dotted line in the occurrence of islands. The arrows show the half width of islands. ($\overline{N}_e$ ~ 1.2 X$10^{19}m^{-3}$, I_p ~140 kA, B_t ~1.5T, q_a~3.5, m/n=3/1 island).

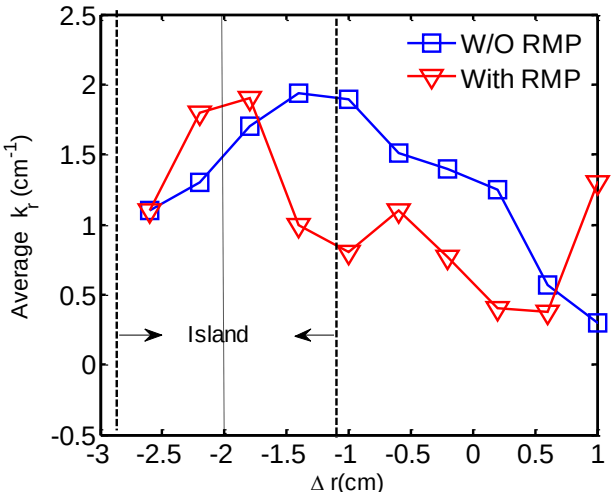

Figure. 14 (color online) The radial profiles of the averaged radial wave numbers of turbulence with and without m/n=3/1 RMPs . (N_e~2.0x10^{19}m^{-3}, I_p~140kA, B_t~1.5T, q_a~3.5, I_{rmp}=3kA, m/n=3/1 island)

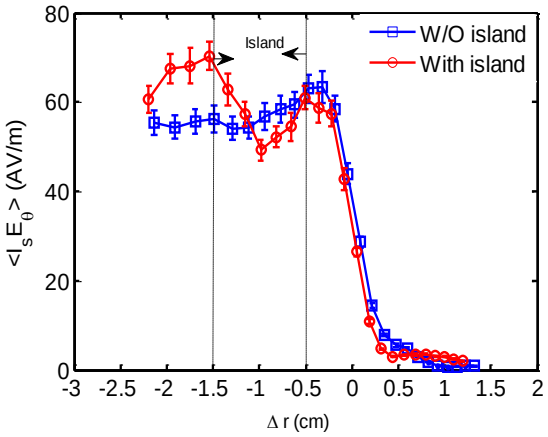

Figure. 15 (color online) Radial profiles of $< \delta I_s \delta E_\theta >$ with and without islands. (N_e~2.2x$10^{19}m^{-3}$, I_p~150kA, B_t~1.5T, q_a~4.3, I_{rmp}=5kA, m/n=4/1 island)

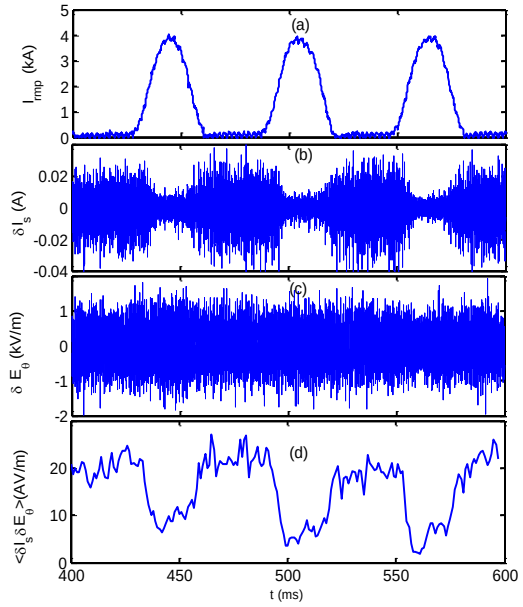

Figure. 16 (color online) $< \delta I_s \delta E_\theta >$ is reduced with RMPs, (a) RMP current, (b) ion saturation fluctuation, (c) poloidal electric fluctuation and (d) $< \delta I_s \delta E_\theta >$. ($\overline{N}_e$~ 1.2 X$10^{19}m^{-3}$, I_p ~140 kA, B_t ~1.5 T, q_a~3.5, m/n=3/1 island)